PLASMONIC NANOSTRUCTURES: FABRICATION AND OPTICAL CHARACTERIZATION

by

SARATH CHANDRA SAMUDRALA

Presented to the Faculty of the Graduate School of

The University of Texas at Arlington in Partial Fulfillment

of the Requirements

for the Degree of

MASTER OF SCIENCE IN PHYSICS

THE UNIVERSITY OF TEXAS AT ARLINGTON

August 2008

ACKNOWLEDGEMENTS

I would like to take this opportunity to thank those who have supported me in carrying out this research. I am very grateful to Prof Michael Vasilyev for giving me this wonderful opportunity to work with him in his group. It was a great learning experience for me. Working with him, I improved many skills from understanding complex ideas, to attaining perfectionism in the given job. And also I like to specially thank him for providing me RA during my thesis work and advising me with patience.

I like to thank Prof Alex Weiss for accepting my request to be my co-supervisor from physics department.

I also like to thank Prof Nail Fazleev for accepting my request to be a member in my thesis committee.

I like to thank my father Dr Manohar , mother Sharada and my brother Subhash Chandra for constantly encouraging me during my entire graduate study.

I like to specially thank my wife Kalyani for her support and encouragement during my research.

I like to thank my group members Pallavi Patki and Muthiah Annamalai for their suggestions and help during my stay in nonlinear optics and nanophotonics laboratory.

June 27, 2008

ABSTRACT

PLASMONIC NANOSTRUCTURES:

FABRICATION AND OPTICAL

CHARACTERIZATION

SARATH CHANDRA SAMUDRALA, M.S.

The University of Texas at Arlington 2008

Supervising professor: Michael Vasilyev

Resonant light localization by metal nanostructures has potential for applications in cavity quantum electrodynamics (e.g. single-photon sources, quantum gates etc) and nonlinear optics.

In this thesis we present the details of fabrication of metal nanocavities in silver films deposited on glass substrates. We discuss the details of the thin film deposition techniques which we used as well as the focused ion beam milling method for drawing nanopatterns on silver films. We also present our studies on optical characterization of gold nano particles on glass substrate showing surface plasmon resonance. We present our theoretical model of this phenomenon using Mie theory and compare it to our experimental results.

TABLE OF CONTENTS

LIST OF ILLUSTRATIONS

LIST OF TABLES

CHAPTER 1

INTRODUCTION

1.1 Introduction

Plasmonics is the field studying the surface plasmon polaritons or surface plasmons on metal dielectric interfaces. These are the collective coherent oscillations of electrons on the surface of metals when light of proper wavelength excites them. This field has recently gained tremendous interest after the discovery in 1998 by Ebbessen et al [1], which showed the extraordinary transmission of light (EOT) by a perforated metallic film. Also it is known that metallic nanoparticles whose sizes are smaller than the wavelength of light, can sustain resonant modes that manifest themselves as hugely increased absorption and scattering cross-sections at specific frequencies at visible and near infrared frequencies of the spectrum. These resonances have been identified as dipole like surface plasmons resonance [2]. Hence the field of plamonics, which is also a sub- field of nanophotonics, has attracted many researchers to use surface plamons for making functional photonic devices with Au and Ag. The development of modern tools and techniques such as electron beam lithography (EBL) and focused ion beam (FIB) systems for the fabrication of nanostructures in metals and dielectrics enhanced the rapid growth of plasmonics research in recent years.

The work in this thesis is aimed at fabricating nano structures for achieving near field confinement and far field beam shaping of light using sub-wavelength slits because of the excitation of surface plasmons. Also this thesis is aimed at discussing our results of modeling and experiments showing the surface plasmon resonance on metallic nanoparticles. First part of thesis discusses the theory and fabrication issues of nanocavities on Ag on glass films. The later part discusses the experimental observation of scattering of light by gold nanoparticles, which we have modeled as Mie scattering.

According to the scalar diffraction theory, the transmittance through subwavelength aperture in an opaque screen is extremely small and is related to the ratio of aperture size to the wavelength. In addition, when the aperture size is smaller than the wavelength of light, the light is diffracted in all directions and only a small fraction of it can be captured by the detector. However, in 1998 the scientific community was greatly surprised by the results of extraordinary transmission of light by holes of sub wavelength dimensions [1]. This paper reported that when light is shined upon subwavelength holes in a metallic film, forming a two dimensional array, the transmission of light through this structure is greatly enhanced at some particular wavelength. The wavelength peaks were found from the dispersion relation of surface plasmons modes running on the metal surface. Hence it was clear that the enhanced transmission is because of the excitation of surface plamons on the surface.

In 2002 it was also reported [3] that extraordinary transmission of light was possible with a single sub wavelength aperture when the surface around the aperture

contained periodic corrugations. Moreover paper [3] reported strong directionality of light at the output of such a structure. This is explained by the generation of surface plasmons on the metal dielectric interfaces the condition is to have a periodic structure on the surface to facilitate the conservation of energy and momentum during coupling of light to plasmon. This effect was observed only for '*p*'- polarized light, i.e. TM waves but not for '*s*'-polarized light.

We are fabricating the nanoaperture structure in silver films on glass substrates. The reason for choosing silver is because it has the highest reflectivity in visible and near infrared ranges among metals. The rectangular or circular aperture in metal film can serve as a metal-clad nanocavity containing light between the input and output faces of the film (each face providing nearly 100% reflection due to the mismatch with free space impedance). Using silver film gives highest quality factor (Q) for our nanocavity. Our future application of this nanostructure is to make single photon emitters. The spontaneous emission properties of an active medium like quantum dot, which we propose to put in the nanocavity, will be modified as it interacts with only one vacuum mode enabling the realization of a deterministic single photon source. For this, we need highest Purcell factor (enhancement of the spontaneous emission into the nanocavity mode), which is given by $F = \frac{3\lambda^3 Q}{2\pi^2 V}$ [4] where Q is the quality factor of the cavity and V is the mode volume. The quality factor directly affects the photon life time in the cavity. Although high value for Purcell factor could be achieved in the cavities based on dielectric micro disks (utilizing the phenomenon of whispering gallery modes) and

photonic crystals, using metallic nanocavities gives the tightest known field confinement leading to unprecedented control over the light matter interactions for *cavity quantum electrodynamics* (QED). The surface plasmon effect of the corrugated structures enables the efficient interface between the nanocavities and optical fibers waveguides and detectors.

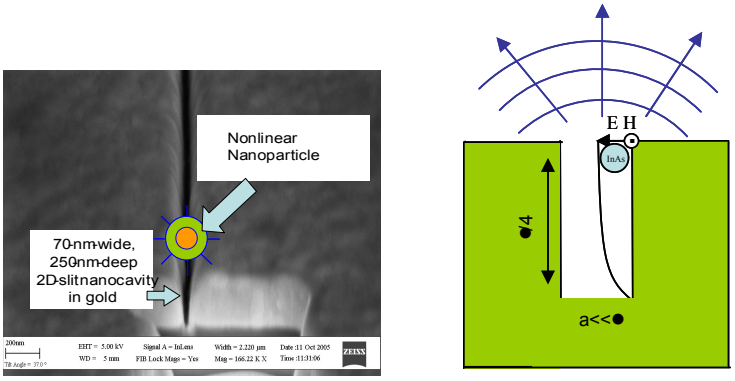

Figure 1.1 Illustrations. (a)Quantum dot in a nanocavity. (b) Quantum dot placed at maximum of vacuum mode.

These metallic structures can confine light to extremely small volumes ($V<<\lambda^3$) with finesses on the order of 10^2. One potential structure hast one end of the cavity short circuited and the other end open. The important factor is that this cavity has the fundamental mode TE_{101} which does not have a cut-off, i.e. can exist in a cavity in which one dimension can be arbitrarily small dimensions. Light emitted from such a cavity is diffracted in all directions. However periodic corrugations made at the exit side of the structure concentrate the light in to a narrow beam with divergence less than 6^0 [3].

The theoretical model for this structure is based on work by Martin-Moreno et al [5,6]. Our group including the author of this thesis has extended this approach to calculate and optimize the coupling efficiency between the Gaussian cavity mode and metal nanoaperture [7,8]. The light emitted from the nanoaperture depends upon geometrical factors of the structure, such as the number, periodicity and depth of the corrugations. The optimization was reported in detail in [9].

In this thesis we discuss the theory behind the electromagnetic field confinement by the nanocavity and the fabrication details of the structure. The nanopatterning is done by focused ion beam (FIB) milling process. A high-intensity beam of Ga^+ is impinged upon the structure with beam waist around 5 nm. The high energy beam etches out the metal in the desired pattern and to desired depth, making the grooves and the cavity. This process step requires considerable optimization of the beam current and the etching time. Also the quality of the thin silver film is very important in making sure that the grooves are perfectly straight and the walls are vertical. We report the initial results of nanocavity fabrication in the films prepared by several different deposition methods.

Another topic of this thesis (discussed in chapter 4) is the plasmonic resonance phenomenon seen in gold nanoparticles with diameters significantly smaller than the wavelength of light. The spectral response of such nanoparticles showed pronounced red shift and substantial broadening as the particles sizes increase. Resonance effect is dependent upon the size, shape and dielectric environment around the nanoparticles. We have experimentally verified the resonance shifts of the scattered light. We have

modeled this effect using the Mie scattering phenomenon by metallic sphere [10]. A MATLAB program is written to calculate the Mie coefficients and the scattered intensity of the light for different wavelengths of light. Our model shows clear resonance, shift towards longer wavelength as the particle size increases, which is in agreement with our experimental results.

CHAPTER 2

PLASMONICS WITH RESONATING NANOCAVITIES

2.1 Introduction

In this chapter the electromagnetic theory in nanocavity, describing light emission from sub wavelength apertures due to surface plasmon resonance (SPR) is discussed. In the experiment we fabricate a metallic nanocavity and propose to put a light emitter in the nanocavity so that it interacts with only vacuum electromagnetic mode. Basically, this cavity is a metallic waveguide with one end short circuited. Hence in this chapter Drude theory of metals, the basic electromagnetic wave modes in slab waveguides, rectangular waveguides and metallic cavities as well as sub wavelength optics due to plasmon resonance are briefly reviewd..

2.2 Drude theory of metals and surface plasmons

Surface plasmons on the metal dielectric interfaces are explained as the collective oscillations of the electrons. The electrons in the metals are described by Drude's model.

In this Drude's theory the atoms condensed into a solid give up their loosely bound valence electrons, which are free to wander through the metal and lead to conduction of charge and energy. The collective valence electrons are treated as an electron gas. The basic assumptions for this model are 1) The electrons flowing in the metal do not interact with other electrons, which is also known as independent electron

Approximation, 2) The electrons experiences collisions with ion cores and suffer an abrupt change in their velocity with a probability per unit time $1/\tau$ .The time τ is called the relaxation time or collision time which is a very important parameter.

The complex dielectric function of a metal given by drude model [11] is as follows

$$\varepsilon = \varepsilon_1 + i\frac{\sigma}{\omega\varepsilon_0} \tag{2.1}$$

The equation above assumes monochromatic traveling wave $e^{i(\vec{k}.\vec{r}-\omega t)}$

Relating collision frequency $1/\tau$ to the electron mobility $\mu = e/m\nu$, equation 2.1 can be written as

$$\varepsilon = \varepsilon_1 - \frac{n_e e^2}{m\varepsilon_0(\nu^2+\omega^2)} + i\frac{n_e e^2 \nu}{m\varepsilon_0\omega(\nu^2+\omega^2)} \tag{2.2}$$

$$= \varepsilon' + i\varepsilon'' = (n+i\kappa)^2 \tag{2.3}$$

$$\sigma = \frac{\sigma_0}{1 - i\frac{\omega}{\nu}} \tag{2.4}$$

ε_1 is the contribution of bound electrons, ν is the collision frequency of the electrons in the lattice, $\sigma_0 = \frac{n_e e^2}{m\nu}$ is the DC conductivity, and n_e,e and m are the charge,concentration and mass of the electrons, respectively. At optical frequencies $\nu << \omega$ and

$$\varepsilon \approx \varepsilon_1 - \frac{n_e e^2}{m\varepsilon_0\omega^2} + i\frac{n_e e^2 \nu}{m\varepsilon_0\omega^3}$$

(2.5)

$$= \varepsilon_1 - \left(\frac{\omega_p}{\omega}\right)^2 + i\left(\frac{\omega_p}{\omega}\right)^2 \frac{\nu}{\omega} \tag{2.6}$$

$$\sigma \approx \varepsilon_0 \left(\frac{\omega_p}{\omega}\right)^2 (\nu + i\omega) \tag{2.7}$$

where $\omega_p = \sqrt{\frac{n_e e^2}{m\varepsilon_0}}$ is the plasmon frequency.

A uniform electron gas can sustain a charge density oscillation. A disturbance caused in the charge density will be sustained and is oscillatory. Then nature of this charge density waves is the plasmon oscillation or plasmons. This has a longitudinal motion.

Surface plasmons are surface electromagnetic waves that have intensity maximum at the surface and decay as they propagate into the material. In our experiment we used silver and glass interfaces.

Surface plasmons propagate with frequencies ranging from ω=0 to ω =$\omega_p/\sqrt{2}$ on metallic films depending upon the '*k*" vector. Their dispersion relation ω (*k*) lies off the light line which says that plasmons are non-radiative.

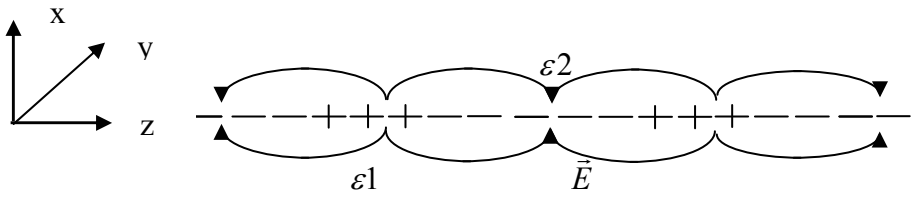

Figure 2.1 Illustration of surface plamons at an interface

The wave vector of surface plasmons is descried as $k_x = \frac{2\pi}{\lambda_p}$. The continuity of electric and magnetic fields at the surface of the metal-dielectric interface are descried as

$$E_{x1} = E_{x2}$$
$$E_{z1} = E_{z2} \tag{2.8}$$

$$H_{y1} = H_{y2} \tag{2.9}$$

Using the Maxwell's equation

$$\frac{\partial H_{y1}}{\partial z} = i\varepsilon_1\varepsilon_0\omega E_{x1} \tag{2.10}$$

and

$$\frac{\partial H_{y2}}{\partial z} = i\varepsilon_2\varepsilon_0\omega E_{x2} \tag{2.11}$$

Looking for solutions in the form of $e^{-k_{z1}z}$ and e^{kz_2z}

$$k_{z1}H_{y1} = -i\varepsilon_1\varepsilon_0\omega E_{x1} \tag{2.12}$$

$$k_{z1}H_{y1} = i\varepsilon_2\varepsilon_0\omega E_{x2} \tag{2.13}$$

(2.14)

From above we get $H_{y1} - H_{y2} = 0$

$$\frac{k_{z1}}{\varepsilon_1}H_{y1} + \frac{k_{z2}}{\varepsilon_2}H_{y2} = 0 \tag{2.15}$$

For these two linear equations, for a solution to exist the determinant has to be zero which can be written as

$$\frac{k_{z1}}{\varepsilon_1} + \frac{k_{z2}}{\varepsilon_2} = 0 \tag{2.16}$$

Solving for k_x we can write

$$k_x = \frac{\omega}{c}\left(\frac{\varepsilon_1 \varepsilon_2}{\varepsilon_1 + \varepsilon_2}\right)^{1/2} \tag{2.17}$$

In this experiment $\varepsilon 1$ is the dielectric function of the silver and $\varepsilon 2$ is the dielectric function of the glass.

2.3 The problem

. In our experiment we are fabricating a nanostructure which is similar to the following figure.

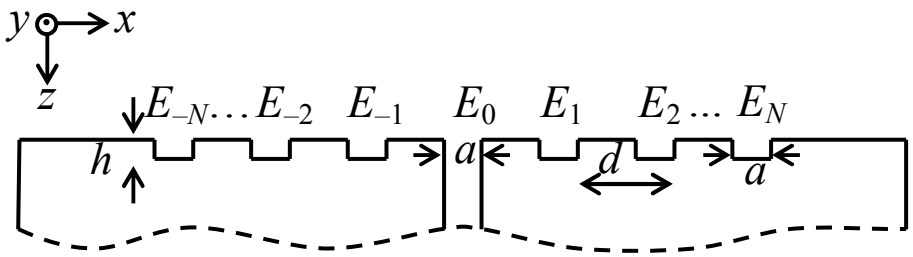

Figure 2.2 Schematic of the nanostructure

The bottom part is a glass wafer. On that glass sustrate silver of thickness 300 nm is deposited. The silver coating is put under focused ion beam milling process to make grooves on the surface. The central groove goes all the way down to the glass surface. The other grooves are drawn symmetrically on either side of the central groove. When the light is input from below through the slit, a concentrated beam of light can be obtained at the output above. The dimensions of this structure are given as follows [5] .

N=10, a=40 nm, d=500 nm, h=100 nm

This structure is designed for a wavelength of λ=560 nm.

The scattering of light from the corrugated surface is given by the following set of equations [5].

$$(G_{\alpha\alpha} - \varepsilon_\alpha)E_\alpha + \sum G_{\alpha\beta}E_\beta = 2i\eta \int_{-\infty}^{\infty} \phi_\alpha^{\,*}(x)H_{in}(x)dx \quad \text{from free space to slit} \tag{2.18}$$

$$(G_{\alpha\alpha} - \varepsilon_\alpha)E_\alpha + \sum G_{\alpha\beta}E_\beta = 2i\eta A_0\delta_{\alpha 0} \quad \text{from slit to free space} \tag{2.19}$$

Both these equations yield the same

$$E(x)\big|_{z=0} = \sum E_\alpha \phi_\alpha(x)$$

$$\text{if } H_{in}(x) = -\frac{A_0}{\eta}\phi_0(x) \tag{2.20}$$

where

$$\eta = \sqrt{\frac{\mu_0}{\varepsilon_0}} = 377\Omega \tag{2.21}$$

$$\varepsilon_\alpha = \frac{1}{\tan kh}, \alpha \neq 0 \tag{2.22}$$

$$\varepsilon_\alpha = -i, \alpha = 0$$

$$\phi_\alpha(x) = \frac{1}{\sqrt{a}} \text{ in groove slit} \tag{2.23}$$

otherwise,

$$\phi_\alpha(x) = 0$$

$$G_{\alpha\beta} = \frac{ik}{2}\int_{-\infty}^{\infty}\int_{-\infty}^{\infty} \phi_\alpha(x)H_0^{(1)}(k|x - x'|)\phi_\beta(x')dxdx' \tag{2.24}$$

The $G_{\alpha\beta}$'s are the Green's functions. Since these equations for many slits can be written in the form of a matrix, the inverse of the Greens function matrix multiplied with input light gives the values of the electric filed vectors at the corrugations. From these, the poynting vector gives the output light intensity.

The center slit forms a rectangular metallic cavity for the light incident on the structure.

Below we provide a brief overview of the fundamental modes existing in the metallic waveguides and cavities in 2 and 3 dimensions.

2.4 Waveguides and resonating cavities

Guided electromagnetic waves along uniform systems are classified in the following way [11]:

TEM waves: The EM waves for which electric and magnetic fields have no components in the propagation direction are called transverse electromagnetic waves.

TM waves: Waves that contain no magnetic field component in the direction of propagation are called transverse magnetic waves components.

TE waves: Waves that have no electric field component in the direction of propagation. These are known as transverse electric waves.

2.4.1Parameters responsible for attenuation of waves

Skin depth (1/e penetration depth of electric field) is given by

$$\delta = 1\Big/\mathrm{Re}(\sqrt{-i\omega\mu_0\sigma}) \approx \frac{1}{\mathrm{Re}\left(\frac{\omega_p}{c}\sqrt{1-i\frac{\nu}{\omega}}\right)} \approx \frac{c}{\omega_p} \qquad (2.25)$$

for $\nu << \omega$.

However the losses in cavities and waveguides are determined by surface resistance R_s, which is a real part of the surface impedance

$$Z_s = \sqrt{\frac{-i\omega\mu_0}{6}} \approx \sqrt{\frac{\mu_0}{\varepsilon_0}}\frac{\omega}{\omega_p}\left(\frac{\nu}{2\omega} - i\right),$$

$$\text{i.e. } R_s \approx \sqrt{\frac{\mu_0}{\varepsilon_0}}\frac{\nu}{2\omega_p} = \frac{1}{2}\frac{e}{\sigma_0}\sqrt{\frac{n_e\mu_0}{m}} \tag{2.26}$$

Assuming (for silver) n_e=5.85 x 0^{28}m^{-3} and $\sigma_0 = 6.17x10^7$ s/m, we obtain R_s=0.37 Ω

2.4.2 TEM waves

One of the simplest wave guiding systems for analysis is that formed by a slab of dielectric with parallel plate conductors on top and bottom. The fields are assumed to be same as if the plates are of infinite width.

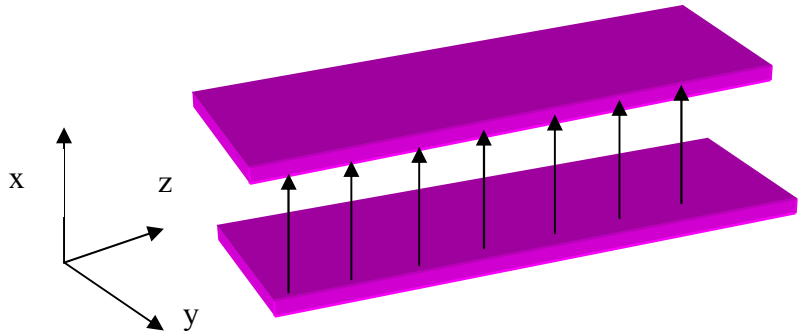

Figure 2.3 Representation of TEM waves as static fields

The fundamental mode of this metal slab waveguide is the TEM mode.

$$E(\vec{z},t) = E_x \hat{x} e^{i(kz\mp\omega t)}, H(\vec{z},t) = H_y \hat{y} e^{i(kz\mp\omega t)} \tag{2.27}$$

where the constant field magnitudes are related by

$H_y = \pm\sqrt{\frac{\varepsilon\varepsilon_0}{\mu\mu_0}}E_x$, with upper sign used for $+z$ traveling wave and lower sign for $-z$ traveling wave. Note that TEM mode does not have a cut off and does not depend on the width *'a'* of the waveguide.

2.4.3 Attenuation in metal slab waveguides

For a slab waveguide of width 'a', the field decays with distance z as

$$E_x(z) = E_0 e^{-\frac{\alpha z}{2}} \tag{2.28}$$

$$\alpha = \frac{2R_s}{\eta a}, \tag{2.29}$$

$$\eta = \sqrt{\frac{\mu_0}{\varepsilon_0}} = 377\Omega$$

For silver $$E_x(z) \approx E_0 e^{-0.001 z/a} \tag{2.30}$$

2.4.4 Rectangular waveguides

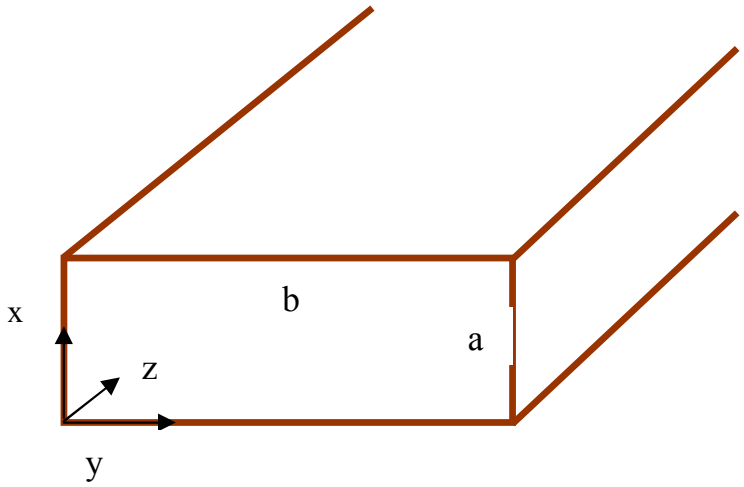

Figure 2.4 Rectangular waveguide

The above figure represents a rectangular waveguide with conducting boundaries on four sides. As we know in such a hollow waveguide TEM waves can not exist .Hence in this structure only TE and TM waves exist. The fundamental mode of the rectangular waveguide is TE_{10}.

2.4.5 TE_{10} wave in a rectangular waveguide

TE_{10} is the fundamental mode in the rectangular waveguide. This mode is independent of one of the dimensions, hence a waveguide can be made to support only TE_{10} mode. The expressions for TE_{10} wave in rectangular waveguide is given below with k_x=0 and $k_c = k_y = \pi / b$

$$H_z = A\cos k_y y, \tag{2.31}$$

$$E_x = \frac{i\omega\mu_0 A}{k_y}\sin k_y y, \tag{2.32}$$

$$H_y = \frac{i\beta A}{k_y}\sin k_y y, \tag{2.33}$$

Where A=const and $\beta = k\sqrt{1-\left[\frac{\omega_c}{\omega}\right]^2}$ is the propagation constant in the z direction. Then

$$E_x = Z_{TE}H_y = E_0\sin(\frac{\pi y}{b}), \tag{2.34}$$

$$H_z = -\frac{iE_0}{\eta}(\frac{\lambda}{2b})\cos(\frac{\pi y}{b}), \tag{2.35}$$

where

$$E_0 = \frac{i\omega\mu A}{k_y} = \frac{i2\eta bA}{\lambda} \tag{2.36}$$

$$Z_{TE} = \eta\left[1-(\frac{\omega_c}{\omega})^2\right]^{-1/2} = \eta\left[1-(\frac{\lambda}{2b})^2\right]^{-1/2}, \tag{2.37}$$

where $\eta = \sqrt{\frac{\mu\mu_0}{\varepsilon\varepsilon_0}}$, $\lambda = \frac{c}{\nu\sqrt{\varepsilon\mu}}$, $\nu = \frac{\omega}{2\pi}$, and

Cut off frequency, wavelength and wave number are

$\nu_c = \frac{c}{2b\sqrt{\mu\varepsilon}}$, $\lambda_c = 2b$ and $k_c = \frac{\pi}{b}$ respectively

2.4.6 Attenuation in rectangular waveguide

In the presence of loss, the fields decay with z as $e^{-\frac{\alpha z}{2}}$

where $$\alpha = \frac{2R_s}{\eta a\sqrt{1-(\frac{\lambda}{2b})^2}}[1+\frac{2a}{b}(\frac{\lambda}{2b})^2] \quad (2.38)$$

In particular for $b = \frac{\lambda}{\sqrt{2}}$,

we have $$\alpha = \frac{2\sqrt{2}R_s}{\eta a}(1+\frac{a}{b}) \approx \frac{2\sqrt{2}R_s}{\eta a} = \sqrt{2}\alpha_{TEM} \text{ for } a<<b \quad (2.39)$$

2.5 Fundamental mode in a metal nanocavity

The metal nanocavity that we fabricated is basically a rectangular waveguide which is short circuited at one end with opening at other side. Hence in this structure, a standing wave pattern is developed. Such a structure is called as a cavity resonator. This cavity supports a standing wave when $\beta L = \frac{\pi}{2}$ i.e. the length of the cavity L is quarter of the wavelength (λ_g in the rectangular waveguide). The analysis of the cavity resonators require the solution of Maxwell's equations subject to the boundary conditions on the cavity walls.

The fundamental mode in the nanocavity is TE_{101} mode. In this mode the *E* field varation in the *y* direction is half-sine, with no variation in the *x* direction with electric field oriented in the *x*-direction and propagating in the *z* direction. For cavity short-circuited on both ends, the condition $E_x = 0$ at $z=0$ and $z=L$, as required by the perfect conductors is satisfied if $\beta L = \pi$,i.e.

$$L = \frac{\lambda_g}{2} = \frac{\lambda}{2\sqrt{1-(\frac{\lambda}{2b})^2}} \ , \tag{2.40}$$

$$\lambda = \frac{2bL}{\sqrt{b^2 + L^2}} \tag{2.41}$$

Then fields in such a nanocavity are described as follows

$$E_x = E_0 \sin\frac{\pi y}{b}\sin\frac{\pi z}{L} \tag{2.42}$$

$$H_y = -\frac{iE_0}{\eta}\frac{\lambda}{2L}\sin\frac{\pi y}{b}\cos\frac{\pi z}{L} \tag{2.43}$$

$$H_z = \frac{iE_0}{\eta}\frac{\lambda}{2b}\cos\frac{\pi y}{b}\sin\frac{\pi z}{L} \tag{2.44}$$

The electric field passes vertically from top to bottom, entering top and bottom normally and becomes zero at side walls as required by the perfect conductor. The magnetic field lines lie in horizontal *(y-z)* planes and surround the vertical displacement current resulting from time rate of change of E_x.

The quality factor of the nanocavity is the most important factor in this experiment. For future single-photon light sources that we propose to work on, the efficiency depends upon the quality factor. One definition for the quality factor is $Q = \frac{2\pi W_s}{W_L}$, W_s is the stored energy in the cavity and W_L is the energy lost in one oscillation. This can be expressed in frequency domain as the ratio of light frequency ν_0 to the full width at half maximum $\Delta\nu_{FWHM}$ of the cavity resonance:

$$Q = \frac{\nu_0}{\Delta\nu_{FWHM}} \tag{2.45}$$

The quality factor is given in terms of surface resistivity R_s as

$$Q = \frac{\nu_0}{\Delta\nu_{FWHM}} = \frac{\pi\eta}{4R_s}\left[\frac{2a(b^2+L^2)^{3/2}}{bL(b^2+L^2)+2a(b^3+L^3)}\right] \tag{2.46}$$

Let us consider two important cases.

a) $L>>a, b$

$$Q = \frac{\pi\eta}{4R_s}\left[\frac{2a\sqrt{(b^2+L^2)}}{bL}\right] \approx \frac{\pi\eta}{2R_s}\frac{a}{b} \tag{2.47}$$

If $b \approx \frac{\lambda}{2}$ (near the cut off) then,

$$Q = \frac{\pi\eta}{R_s}\frac{a}{\lambda} \tag{2.48}$$

For $\frac{a}{\lambda}$=1/10, the obtained Q value is 314.

b) The smallest short-circuited cavity has $b = L = \lambda/\sqrt{2}$

then $$Q = \frac{\pi\eta}{4R_s}\frac{4a}{\lambda + 2\sqrt{2}a}, \text{ or } Q \approx \frac{\pi\eta}{R_s}\frac{a}{\lambda} \text{ for a} << \lambda \tag{2.49}$$

which is exactly the same as that for the case (a) which indicates that Q does not, at least, significantly, vary with *b* and *L*.

CHAPTER 3

FABRICATION OF METAL NANOCAVITIES

The first step in the fabrication of metal nanocavities is the deposition of silver film on a glass substrate. This is accomplished using physical vapor deposition (PVD) process. A 300 nm thick layer of silver is deposited on a microscope cover glass. The smoothness of the film is very important for further fabrication steps. Hence the theory behind thin film deposition is understood and presented in this chapter. Once the film is made, the quality of the film is studied using SEM (scanning electron microscope) and is analyzed according to the obtained average grain sizes. Once this is accomplished, the nanostructure patterns are drawn on the films using focused ion beam (FIB) method.

3.1 Sample preparation

Before the FIB experiment is done, the sample is made by coating the silver film on 18 x 18mm microscope cover glass (130-170 μm thick). This is carried out in Class 10,000 clean room in Nanofab. Before the actual thin film deposition process, the glass wafer is cleaned with acetone and dried with dry N_2. Once the glass wafer is completely dried, it is taken for deposition process using tweezers.

The required thickness of the silver film is 300 nm. To achieve this we used the well established thin film deposition techniques. We compared the following three techniques to achieve better quality of films.

- Thermal evaporation
- Sputtering
- E-Beam evaporation

Thermal evaporation:

Thermal evaporation involves heating of the material that we want to deposit on our wafer. We have used NRC 703 thermal evaporator in NanoFAB. Silver pellets are put in the tungsten boat. For obtaining 300 nm-thick layer of silver, 6 to 7 silver pellets need to be taken. Initially, rough pumping of the turbo is performed. Once the tungsten boat is fixed between the electrodes, the dome of the chamber is brought down. Once the thermocouple gauge shows pressure in the chamber below 1 mT, turbo is turned on. Now the pressure is measured using ion gauge. The current supply is started once the pressure is below 5 μTorr. Current is gradually increased. Once the desired deposition rate is achieved, the current is maintained constant and the shutter is opened for deposition. At this stage the current should not be increased abruptly as it may cause damage to the boat. Once the desired thickness is achieved, the current is slowly decreased to zero. Once the chamber is vented with dry N_2, the samples are taken out.

Sputtering:

The basic idea behind the sputtering is the momentum transfer. Energetic ions release the atoms from the surface of the target material and the liberated atoms in vapor phase deposit over the substrate. We have used the NanoFAB's home made RF sputtering machine. The target material is a silver disk of 2″ in diameter. This disk is placed on a Cu backing plate to dissipate the heat generated by bombardment of Ar gas ions. Since the sputtered material emanates in a cosine distribution the substrate is placed directly above the target. The substrate is RF biased for the sputtering to happen. Once the discharge starts, the high energy Ar ions strike the target and the vapor phase of the silver is generated, which is deposited on the glass wafer. The proper RF power ensures the uniformity of sputter rate.

E-Beam evaporation:

In this process an intense beam of electrons hit the source material and converts it into vapor phase. In the system that we used the potential drop maintained to generate the electron beam is 12 kv. We have used the CHA e-beam evaporator in the NanoFAB. To avoid the dissolving of the electron emitting filament by the evaporated atoms, the filament is placed out of sight from source. A magnetic field is used to bend the electron beam and direct it onto the source. Hence the electrons in this system experience Lorentz force. The main precaution in this experiment is to make sure that the electrons hit only the source material and not the crucible, in which the silver is placed. The deposition uniformity is improved by scanning the beam around the surface in the raster pattern. Without rastering, the evaporating material tends to be angularly distributed.

We deposited silver using this method which gave us pretty good film quality. However, we encountered the following problem: the films were getting corroded after a few days of being kept in ambient conditions. We suspect the evaporator chamber contamination to be responsible for that. Hence we did not use these films in making the nanocavities.

3.2 Theory behind thin film deposition

Thin film process basically contains four steps. 1. A source material is provided. 2. The material is transported to the substrate. 3. Deposition takes place. 4. Film is analyzed. In this experiment, silver is the source material. The deposition can be performed either by sputtering or by using energetic electrons to remove particles from source or by thermal evaporation of the source material. In all these process there exists a phase in which the solid silver and vapor phase co-exist. The fundamental diagram is the P-T diagram [12] of the material, which can be obtained in data sheets. For a particular substance, at any temperature, there exists a pressure at which the solid phase and vapor phase of the substance exist simultaneously. The source material is converted to vapor phase and again gets condensed back to solid form either at the source or at the film on the substrate.

In the thin film deposition, the pressure in the chamber is usually made less than the vapor pressure of the material at the operating temperature. This is to make sure that the immediate condensation of the generated vapor does not happen.

The vapor deposition process is achieved under an equilibrium condition which can be described in terms of Gibbs free energy or in terms of chemical potential.

Gibbs free energy is given as

$$G = H - TS = U + PV - TS \tag{3.1}$$

where H is the enthalpy, T is temperature, S is entropy, P is pressure and V is volume. Differentiating the above equation, we get

$$dG = dU + pdV + Vdp - TdS - SdT \tag{3.2}$$

From the first law of thermodynamics, we have

$$dQ = dU + pdV \tag{3.3}$$

Hence at constant pressure

$$dQ - dU + pdV = 0 \equiv TdS - SdT - dU + pdV \tag{3.4}$$

At constant temperature equation (3.2) reduces to equation (3.4), i.e.

$$dG = 0. \tag{3.5}$$

This shows that for processes carried out at constant T and P, Gibbs free energy G remain constant. Thin film deposition is the best example of such a process. Hence G provides a concise definition for equilibrium process such as evaporation. The equilibrium condition can also be described in terms of chemical potential. Chemical potential is given as

$$\mu_i = \frac{\partial G_i}{\partial N_i} \tag{3.6}$$

This explains the incremental change in the Gibbs free energy by the addition of material in that phase at constant temperature and pressure. Since Gibbs free energy

remains constant during thin film deposition, the chemical potential of the condensate phase and vapor state of the material remains same.

$$\mu_c = \mu_v \quad , \tag{3.7}$$

$$d\mu_c = d\mu_v , \tag{3.8}$$

$$dG_c = dG_v . \tag{3.9}$$

Then we can write $V_c dP - S_c dT = V_v dP - S_v dT$ or

$$\frac{dP_v}{dT} = \frac{\Delta S}{\Delta V} \tag{3.10}$$

Then

$$\frac{dP_v}{dT} = \frac{\Delta H_v}{T\Delta V} \tag{3.11}$$

This is the Clasius-Claperion equation. Since for ideal gases $\Delta V = \frac{RT}{P}$

We can write

$$\frac{dP_v}{P_v} = (\frac{\Delta H_v}{T^2 R})dT \tag{3.12}$$

The solution for this equation is expressed as

$$P_v = B\exp(-\frac{\Delta_v H}{RT}) \tag{3.13}$$

This gives us an important relationship between the vapor pressure and the temperature. Thus it is very important to estimate the vapor pressure of the material because it directly determines the *'rate of evaporation'* in thin film deposition process.

3.2.1 Evaporation rate

Rate of evaporation is a primary physical factor that directly affects the quality of the film. We have experimented with various evaporation rates and compared the average grain sizes to optimize this parameter. Heinrich Hertz found experimentally that the rate of evaporation is directly proportional to

$$P_v - P, \tag{3.14}$$

where P_v is the vapor pressure and P is the ambient pressure acting on the evaporant in condensed phase. Rate of evaporation cannot be increased by merely supplying more heat to the source unless the equilibrium vapor pressure is also increased by this action. Thus the evaporation is set by P_v. Including the striking coefficient α_v of the vapor molecules on to the surface, which was introduced by Knudsen, the Hertz-Knudsen equation is given by

$$\frac{dN}{Adt} = \alpha_v (2\pi m k_B T)^{-1/2} (P_v - P) \tag{3.15}$$

where A is area of the orifice, k_B is the Boltzman constant, m is the molecular weight and T is the temperature.

This equation determines the rate of evaporation ($\frac{dN}{Adt}$ is # of atoms striking per unit time on unit area).

3.3 Nanopatterning using focused ion beam

Focused ion beam (FIB) system is used for drawing the nanopatterns on the substrate. In this system, a high intensity beam of ions mills the surface to the desired depth to draw a variety of nanoscale structures on metals and semiconductors. This technique has found widespread use in microelectronic circuit repair in which thin films of conductors and insulators less than half a micron may be cut and deposited with precise tolerances. FIB in semiconductor industry is used to insert jumpers or create open circuits at strategic points on an integrated circuit. In this way a chip which is initially faulty may be repaired and salvaged. We employ the FIB technique because of very fine obtainable resolution owing to the small deBroglie wavelength of ions.

3.3.1 Overview of focused ion beam technology

In our experiment we used Zeiss 1540XB crossbeam system that comprises a focused ion beam and a built in SEM. This system is a cross beam system which means it has both an electron gun and an ion gun pointing at same spot. Focused ion beam system uses a liquid metal ion source of Gallium ions. The system processes a column which contains liquid metal ions. It produces and directs a stream of high-energy massive Ga^{+} ions, focusing them onto the sample both for the purpose of etching or milling the surface and as a method of imaging. The ion's large mass allow them to easily expel the surface atoms from their positions and produce secondary electrons from the surface, which enables the ion beam to image the sample before and after lithography process.

The Ga^+ ions are pulled out from the surface by an electric field. They subsequently pass through apertures and are scanned over the sample surface. The ion-atom collision can be either elastic or inelastic. Elastic collision results in the excavation of surface atoms which is essentially sputtering or milling. Inelastic collisions transfer some of the ions energy to the surface atoms or electrons resulting in the emission of secondary electrons used for imaging.

The FIB system has four basic functions. Milling, deposition, implantation and imaging. Milling is a process that allows digging into the sample surface as a result of the use of relatively heavy ions in the beam. It can be converted into a deposition device simply by adding a gas delivery device that allows the application of certain materials, usually metals, to the surface of the material where the beam strikes. Ion implantation is another important component of surface modification that is available using the FIB. In addition to these, FIB also has imaging capabilities.

In all presently available FIB systems, Ga^+ ions are used. The main advantage is that, because of the low melting point (29.8^0C), minimum heating is required, and gallium can be easily kept in liquid phase during the operation. The ions are heavy and thus milling of the hard materials is possible and at the same time they also do not damage the sample. Gallium's low volatility at the melting point conserves the supply of metal and yields a long source life of about 400 μ-A/mg.

3.3.2 The focused ion beam milling process

Once the silver coated glass samples are ready, they are taken to the FIB room where the nanopatterns are drawn on them. First, the sample has to be mounted on a

stage. The edges of the sample have to be coated with a silver paint to avoid the charging effects due to the incoming ions and electrons. This is an important step which needs to be taken care of. If the charging is not done properly, the image will appear either too bright or too dark and using the contrast and brightness knobs would not solve the problem. Once the sample is mounted, it is inserted into the chamber. The air in the chamber has to be pumped out. Once the desired pressure is obtained inside the chamber the electron gun and ion guns can be switched on. The FIB system that we used has both SEM and ion guns. The surface of the sample can be seen first by the SEM. During the focused ion beam operation the screen can switch between FIB and SEM. Once the sample is inside it has to be brought to a tilt at an angle of 54^0, because the ion gun is placed at 54^0 with respect to the electron gun. Now the sample surface will be perpendicular to the ion gun. Then the stage has to be moved closer to the electron gun. After reaching distance of 9-10 mm from electron gun, the surface is imaged. Once the proper area on the sample is chosen for nanopattering, the image of the sample has to be obtained using ion gun also. And it has to be made sure that both SEM and FIB are showing the same point which is the cross beam point. This procedure takes considerable time. One this is achieved, the control is given to the FIB and the pattern will be drawn. Prior to that the stage has to be moved very slowly to a distance of 4-5 mm from the gun. This has to be done with extreme care. It can result in the hitting of the sample with the gun and damaging both the stage and the gun. All the movement of the stage can be seen on the computer screen. The computer screen can be

shifted between three different modes: the CAMERA MODE, SEM MODE and FIB MODE.

Drawing patterns can be done either by CAD software or manually. But in any case the important things are the values of current and etching time. These are the parameters that have to be optimized for obtaining proper depth and width of the structure. We have experimented with various values of current and etching time. For obtaining 300 nm of depth, we used 10 pA of current and 1200 s of milling time. The results of the different currents and milling times are shown in the next section. It is important to note that the higher current implies the larger aperture size. Hence, even for small milling time a groove of 300 nm can be obtained, but the width of the groove will not be narrow. Hence we had to spend considerable amount of time optimizing these parameters.

3.3.3 Focusing and aberrations issues

The aberrations in ion optics or electron optics are similar to those in geometrical optics. The main aberrations in imaging are spherical aberrations, chromatic aberrations and astigmatism. The spherical and chromatic aberrations are the properties of the lenses and apertures that the user of our FIB system cannot change. In our FIB system, the user has the option of reducing astigmatism only. This is an effect of asymmetry in the focusing field, where the cross section of the beam in a given plane is not circular, but rather elliptical, causing the defocused beam to appear elliptical rather than circular. Astigmatism correction is done during the focusing of the image. When the image is being focused if any wobbling behavior is observed, then we need to use the knob

which reduces the astigmatism. Usually, once the astigmatism is minimized, it stays this way during further fabrication process.

The minimum magnification of the SEM in this system is 53X, where as for FIB it is 421X. The focusing has to be done separately when the mode is switched from SEM to FIB. Once the particular magnification is chosen, then the focusing is carried out. Focusing at lower magnifications is easy, but focusing at higher magnification requires good experience with the system. The focus has to be re adjusted as the magnification changes. Hence, as we go for higher magnifications, the focus has to be re-adjusted again. Once the focusing is done at higher magnifications, it is not required to adjust again when the magnification is reduced.

3.3.4 Cross beam point of SEM and FIB

As we have mentioned the FIB instrument also has a built in SEM gun. The image of the sample can be seen either in FIB or in SEM. Measurement of the depth of the groove is easier when SEM is used. Because the SEM gun is at an angle of 54^0 from the FIB. Once the milling is done, the control goes to SEM. To draw next pattern, we need to come back to FIB. If we do not find the cross beam point then the next structure intended to be drawn just next to the initial structure would fall somewhere else. Hence initially a part of the sample is selected for observation of the same spot by both FIB and SEM. Since the minimum magnification of FIB is 420X and the minimum of SEM is 53X, the SEM also has to be brought to 421X magnification.

3.3.5 Measuring the depth of the grooves by milling a trench

Once the groove is drawn, the depth of the groove can be estimated to a good accuracy by user controls in the menu. But for this we need to mill a trench crossing the groove. It is shown in Fig 3.1.

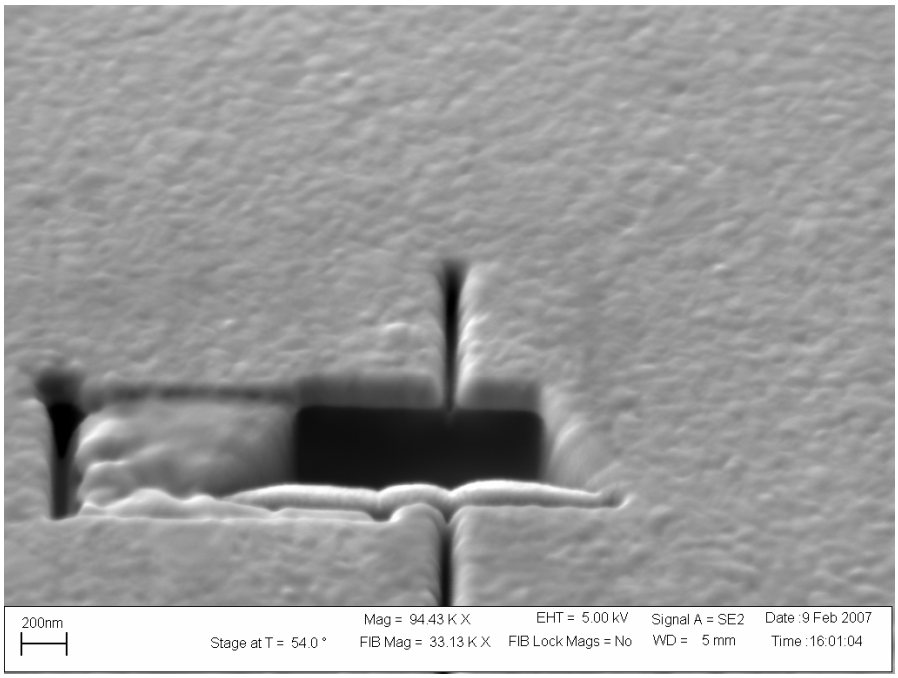

Fig 3.1 Nanogroove with a trench

In milling the structures using focused ion beams, the concern is with the amount of current and the milling time. Higher current leads to wider groves. In the following image the current used was 1 nA for 250 seconds. Even though the obtained depth is near 300 nm the width of the groove is about 1.6 μm (too wide for us).

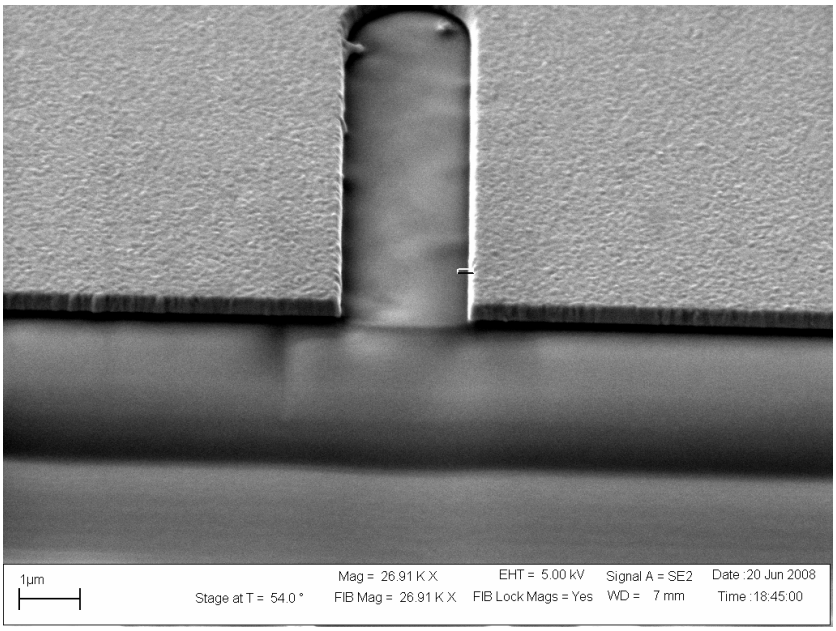

Fig 3.2 Wide groove (width=1.6μm)

Hence if the required width of the groove is small, the best idea is to use very low currents with long milling times. But the trench can be milled with high currents if we are not concerned with the minimizing the widths of the trench. Such trench can be used to find the depth of the groove.

3.4 Results and discussion

We used three different deposition techniques. First, we tried using RF sputtering technique. For this we used the home-made sputtering system. A 2″ diameter silver sputter target was used. When the smoothness of the film was observed under SEM, it was not as desirable as we wanted. Next, we tried the e-beam evaporator. The rate of deposition was varied from 1 to 4 Angstrom/s.

Even though the sample made using e-beam evaporation was smooth (Fig 3.3), we observed the formation of white spots on the sample after a few days of exposure to the atmosphere. As long as the samples were kept in nitrogen box, the sample was not deteiorated. But they started forming a kind of rust when exposed to outside environment. Therefore, we turned to thermal evaporation of the silver. First we used very low deposition rates 0.5-1 A^0/s. But that resulted in the formation of large grain sizes. Fig 3.4 shows SEM image this sample.

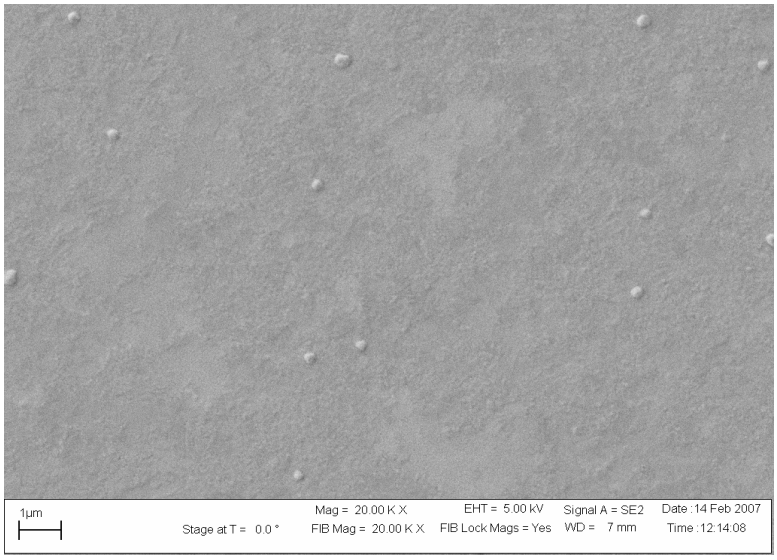

Fig 3.3 SEM image of E-beam evaporated sample

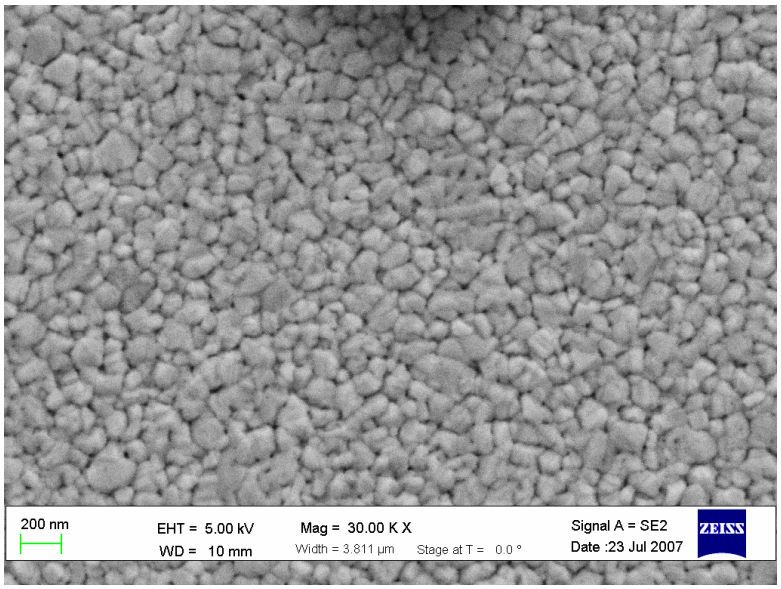

Fig 3.4 Surface morphology of thermally evaporated silver with evaporation rate 0.5-1A^0/s

Thus we had to optimize the deposition rate. This was done and we observed that any value between 2-3 A^0/s was giving a reasonably good morphology. Fig 3.5 is the image of the thermally evaporated silver at 2-3 A^0/s.

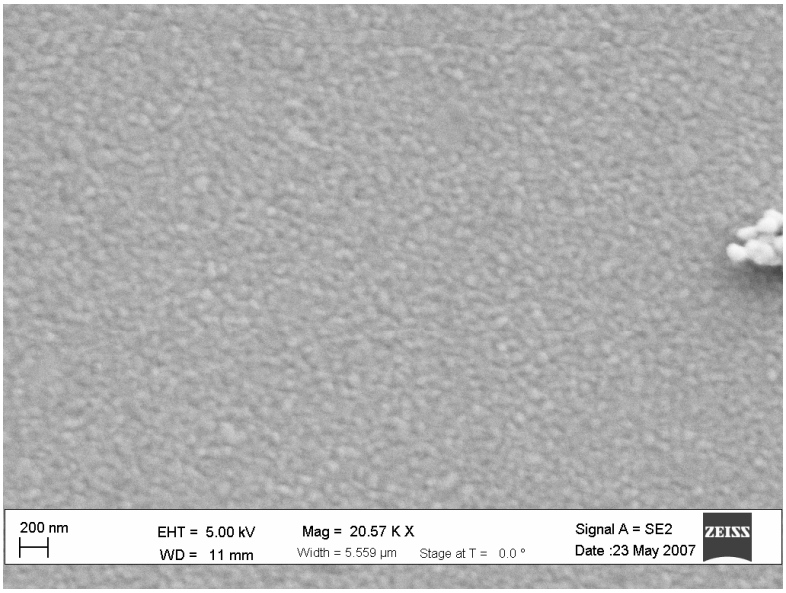

Fig 3.5 SEM image of thermally evaporated sample obtained at 2-3 A^0/s deposition rate.

We used thermally evaporated sample for drawing the nanopatterns on the sample.

As we discussed earlier, current and milling time are the parameters that we tried to optimize. Fig (3.6) shows the nanogroove that is drawn by keeping current constant but varying the milling time.

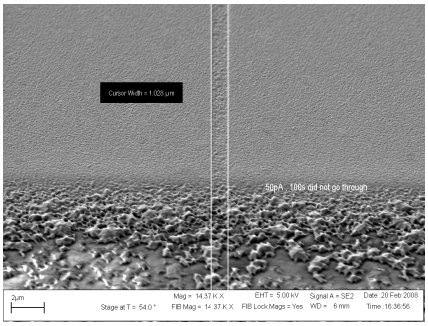

(a)

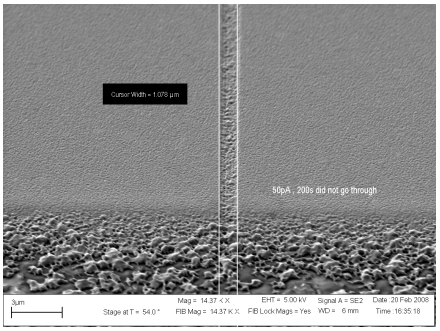

(b)

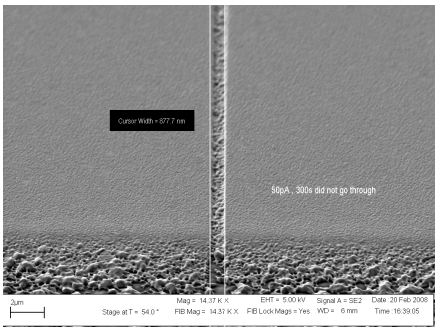

(c)

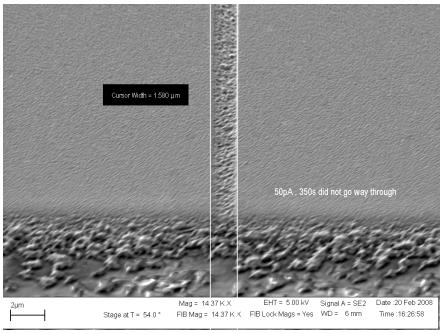

(d)

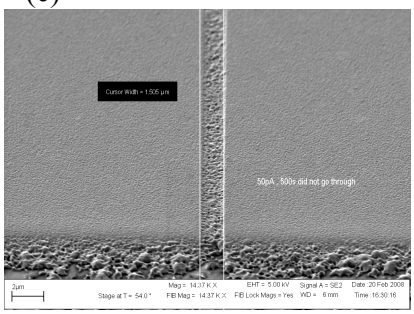

(e)

Figure 3.6 SEM images showing increase in groove width with 50 pA of current and time (a) 100 s (b) 200 s (c) 300 s (d) 350 s (e) 400 s

Table 3.1 Table showing current and milling time.

Fig.3.6	Current	Time
a	50pA	100
b	50pA	200
c	50pA	300
d	50pA	350
e	50pA	400

3.5 Conclusion

We have experimented with three thin film deposition techniques. Optimization of deposition rates is completed and good qualities of films are fabricated. On these samples nanocavities are fabricated using the focused ion beam milling process. The optimizations of FIB parameters for achieving the desired dimensions are understood and results of the experiments are presented.

CHAPTER 4

MODELLING AND OPTICAL CHARACTERIZATION OF GOLD NANO PARTICLES

4.1 Introduction

When metallic nano particles are illuminated by electromagnetic radiation, intense absorption and scattering of light is observed. This is because, these metal nanoparticles can be seen as a resonators for surface plasmons [13]. When the size of the metal nanoparticles is comparable to the penetration depth of electromagnetic radiation, the radiation can shift the free conduction electrons from their ion lattice. To produce surface charges of opposite sign on the opposite surfaces of the particle, this generates a local restoring field within the particle. The coherently shifted electrons of the metal particle together with the restoring field form an oscillator. The resonances of these oscillators are the surface plasmons on the metal nanoparticles.

The scattering of electromagnetic energy is strongly dependent on the wavelength of the incident light. The absorption and scattering are also found to be strongly dependent on the size of the nanoparticles In this chapter we discuss how this phenomenon can be understood and how we modeled it using Mie scattering theory. We also present the comparison of modeling and our experimental results.

4.2 Diffraction by metallic nano spheres:Mie theory

A good analytical treatment for the resonant scattering by nanoparticles can be described by Mie theory for scattering and absorption of light by metallic spheres [10]. G.Mie obtained on the basis of the electromagnetic theory, a rigorous solution for the diffraction of a plane monochromatic wave by a homogenous sphere of any diameter situated in a homogenous medium. The Mie's solution, though derived for diffraction by a single sphere, also applies to diffraction by any number of spheres, provided that they are all of same diameter and composition and are randomly distributed and separated from each other by distances that are large compared to the wavelength. Under these circumstances, there is no coherent phase relationship between the light that is scattered by different spheres, and the total scattered energy is then equal to the sum of the energies that is scattered by different spheres.

The geometry of the problem is represented in Fig 4.1.

Here we consider a linearly polarized plane wave that falls on a sphere of radius 'a' and dielectric permittivity ε^{II}, immersed in a homogenous, isotropic medium, with the permittivity of ε^{I} It is assumed that the sphere is non magnetic and immersion medium is non conducting. The scattered field is nothing but the diffracted field.

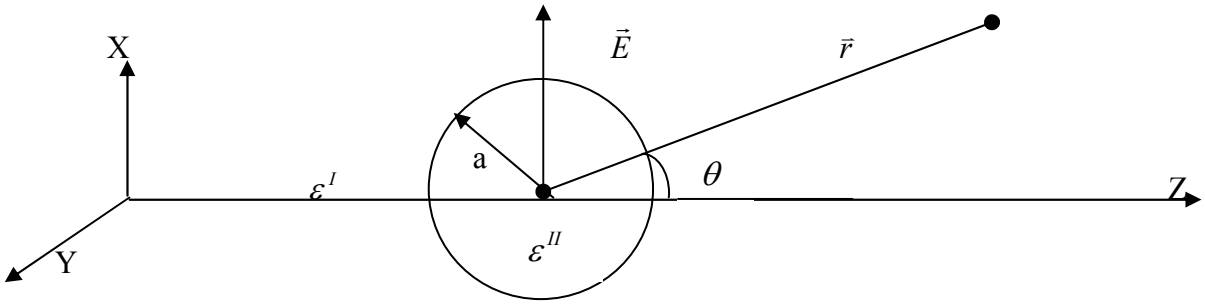

Fig 4.1 Metallic sphere immersed in dielectric constant ε^I

Let the electric vector of the incident electromagnetic field be $E^{(i)}$ and $E^{(s)}$ is that of the scattered field, and $E^{(w)}$ is that of the field within the sphere.

Outside the sphere

$$E = E^{(i)} + E^{(s)} \tag{4.1}$$

Inside the sphere $E = E^{(w)}$ (4.2)

Since the medium surrounding the sphere is assumed to be a non conductor i.e. $\sigma^{(I)} = 0$, then defining the propagation constants in the two regions, we can write

$$k_1{}^{(I)} = \frac{i\omega}{c}\varepsilon^{(I)} = i\frac{2\pi}{\lambda_0}\varepsilon^{(I)} \qquad k_2{}^{(I)} = \frac{i\omega}{c} = i\frac{2\pi}{\lambda_0}, \quad k_1{}^{(I)} = \sqrt{-k_1{}^{(I)}k_2{}^{(I)}} = \frac{2\pi}{\lambda^{(I)}} \tag{4.3}$$

$$k_1{}^{(II)} = \frac{i2\pi}{\lambda_0}(\varepsilon^{(II)} + i\frac{\sigma}{\omega\varepsilon_0}), k_2{}^{(II)} = i\frac{2\pi}{\lambda_0},$$

$$k^{(II)} = \sqrt{-k_1{}^{(II)}k_2{}^{(II)}} = \frac{2\pi}{\lambda_0}\sqrt{\varepsilon^{(II)} + i\frac{\sigma}{\omega\varepsilon_0}} \tag{4.4}$$

where λ_0 is the wavelength of the light in vacuum, and $\lambda^{(I)}$ is the wavelength of the light in the medium surrounding the sphere. For convenience the complex refractive index of the sphere relative to the surrounding medium is represented as n, where

$$n = \frac{k^{(II)} k_2{}^{(I)}}{k^{(I)} k_2{}^{(II)}} = \frac{k^{(II)}}{k^{(I)}}. \tag{4.4}$$

Let us introduce a dimensionless parameter $q = \frac{2\pi}{\lambda^{(I)}} a$.

According to this theory the different eigen modes of the spherical particles are dipolar or multipolar in nature. When the Maxwell's equations are solved using the spherical polar coordinates, we end up with two Mie coefficients.

$${}^{e}B_l = i^{l+1} \frac{2l+1}{l(l+1)} \frac{n\psi_l'(q)\psi_l(nq) - \psi_l(q)\psi'_l(nq)}{n\varsigma_l{}^{(1)'}(q)\psi_l(nq) - \varsigma_l{}^{(1)}(q)\psi_l'(nq)}, \tag{4.6}$$

$${}^{m}B_l = i^{l+1} \frac{2l+1}{l(l+1)} \frac{n\psi_l(q)\psi_l'(nq) - \psi_l'(q)\psi_l(nq)}{n\varsigma_l{}^{(1)}(q)\psi_l'(nq) - \varsigma_l{}^{(1)'}(q)\psi_l(nq)}, \tag{4.7}$$

where $\psi_l(\rho) = \sqrt{\frac{\pi\rho}{2}} J_{l+1/2}(\rho)$ $\varsigma_l{}^{(1)}(\rho) = \sqrt{\frac{\pi\rho}{2}} H^{(1)}{}_{l+1/2}(\rho)$ with

$J_{l+1/2}$ and $H_{l+1/2}$ being Bessel and Hankel functions respectively, and prime symbol standing for differentiating the function with respect to its argument.

Incorporating the Mie coefficients the intensity of the scattered light with polarization parallel or perpendicular to that of the incident wave polarizations respectively.

$$I_{\text{parallel}} = \frac{\lambda^{(I)2}}{4\pi^2 r^2} \left| \sum_{l=1}^{\infty} (-i)^l [eB_l P_l^{(1)'}(\cos\theta)\sin\theta - mB_l \frac{P_l^{(1)}(\cos\theta)}{\sin\theta}] \right|^2, \tag{4.8}$$

and

$$I_{\text{perpendicular}} = \frac{\lambda^{(I)2}}{4\pi r^2} \left| \sum_{l=1}^{\infty} (-i)^l [eB_l \frac{P_l^{(1)}(\cos\theta)}{\sin\theta} - mB_l P_l^{(1)'}(\cos\theta)\sin\theta] \right|^2, \tag{4.9}$$

respectively. Here the $P_l^{(1)}(\cos\theta)$ are the associated Legendre functions of the first kind. Using these equations we can calculate the normalized intensity of the scattered light, which is given by

$$I = \frac{4\pi^2 r^2 (I_{perpendicular} + I_{parallel})}{\lambda^{(I)2}} \tag{4.10}$$

We have written a MATLAB program to simulate the scattering of the light by the gold nano spheres. The sizes of the gold nano spheres we considered are 20 nm, 40 nm, 60 nm ,80 nm and 120 nm. In the MATLAB program we have incorporated the frequency dependent part of the dielectric constant for gold which is taken from reference [6]. A polynomial fit is constructed after taking all the numerical values of the frequency dependent dielectric constant. Both the real and imaginary part of the refractive index are included in the program which uses them to calculate the Bessel functions $\psi^{(I)}$ and Hankel function $\varsigma^{(I)}$ and computes the scattered intensity. This process is repeated for various wavelengths. The Bessel and Hankel function computations are written as functions that are called upon from the main program.

4.3 Results and Discussion

Figures 4.2 and 4.3 below show the atomic force microscope (AFM) and SEM images of randomly scattered gold nanoparticles on silicon dioxide and silicon substrates, respectively.

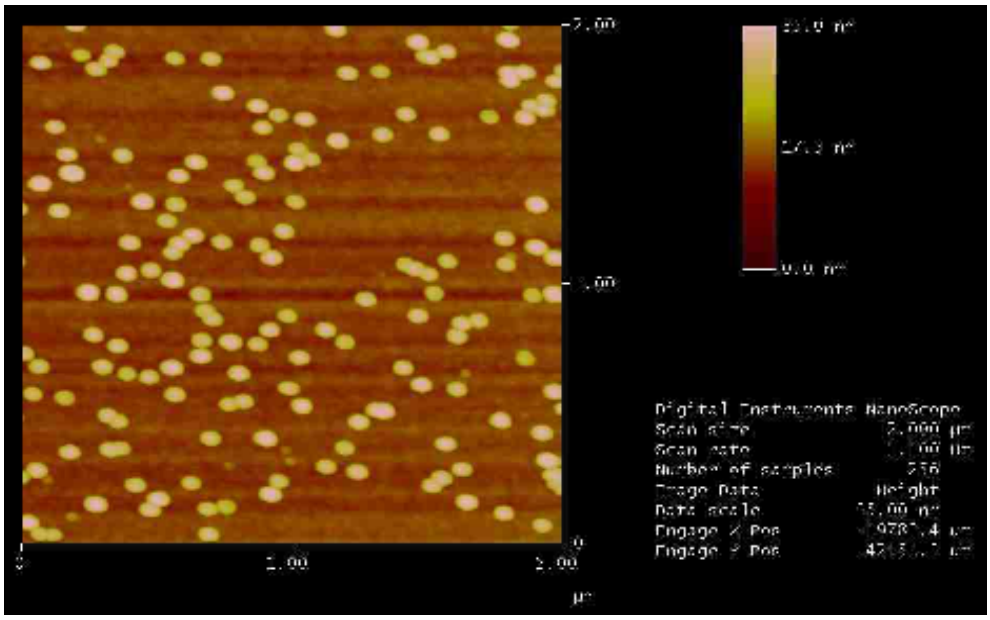

Fig 4.2. AFM image of 20 nm nanoparticles on SiO_2

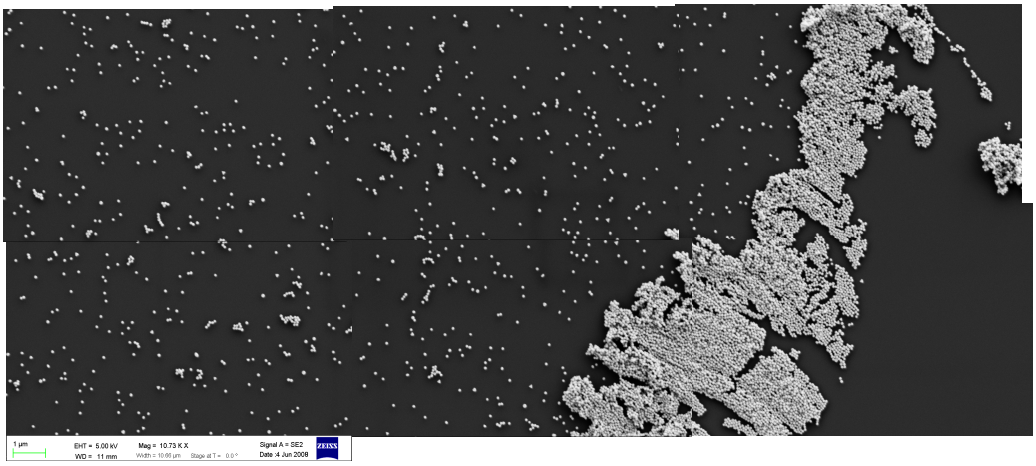

Fig 4.3. SEM image of 80 nm nanoparticles on Si substrate

Figure 4.4 shows the experimental result we obtained by measuring reflectance of the TM polarized light from the samples with different nanopartcile sizes.

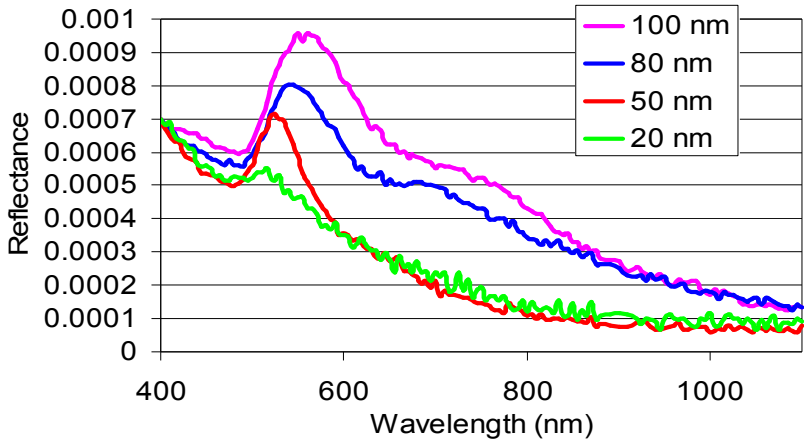

Fig 4.4 Shift in the plasmon resonance wavelength with size of the nanoparticle.

In this experiment a sample with gold nanoparticles deposited on a glass substrate is taken. The sample is studied with an ellipsometer by illuminating it with different wavelengths of light. Since we wanted to reject the light directly reflected from the glass, which creates the back ground signal, we used illumination at Brewster's angle, which is 56^0 in our case.

When we took the spectral response ranging from 400 nm to 1000 nm, we observed strong plasmon resonance peaks which varied with the size of the gold spheres deposited on the sample. The peaks shift towards longer wavelengths as the size of the particles increase, which can be seen in Fig 4.4.

We modeled this phenomenon using Mie scattering theory. Figure 4.5 shows the result of our model. Our model agrees with the experiment by predicting the red shift in the resonance as the size of the particles increases.

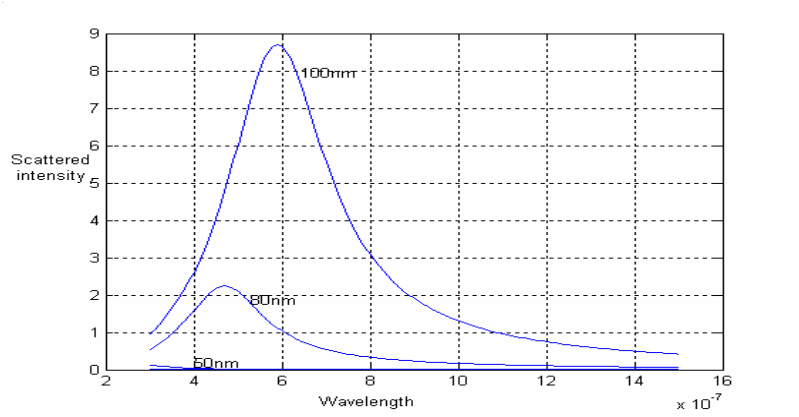

Fig 4.5. Results of Mie theory of gold nanoparticles of sizes 50 nm, 80 nm, 100 nm

In our model we incorporated the complex dielectric constant $\varepsilon = \varepsilon^{(II)} + i\frac{\sigma}{\omega\varepsilon_0}$ of gold.

Figure 4.6 shows the real and imaginary parts of the dielectric constant of the gold [14] with respect to wavelength. Note that the real part of ε is negative in the wavelength range of interest (visible and near infrared), because conductivity σ ,is in turn, also a complex number.

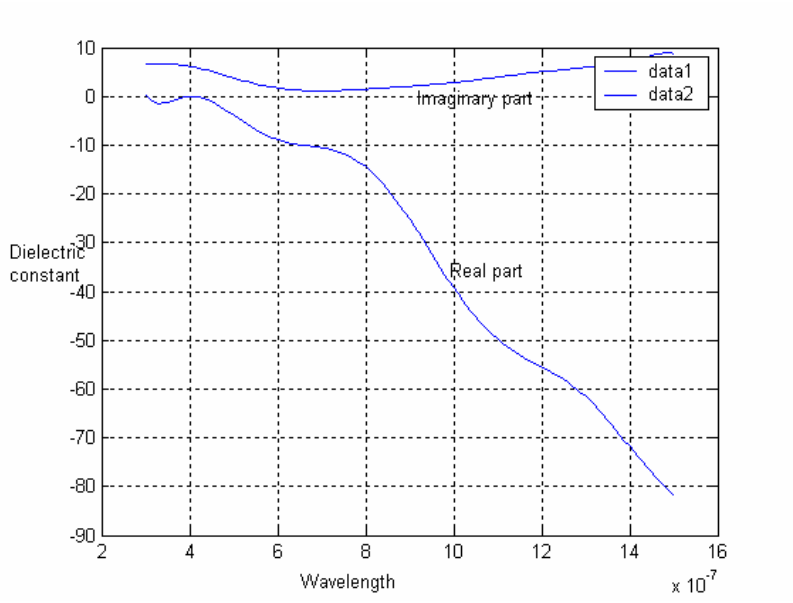

Fig 4.6.Frequency dependent dielectric constant of gold

CHAPTER 5

CONCLUSION AND FUTURE WORK

In this thesis we have presented our fabrication and modeling results on nanostructures benefiting from surface plasmon resonance. To fabricate low loss metal nanocavities,we have optimized the rate of deposition for silver deposition on glass substrates and used focused ion beam milling process.

We also have studied the resonance scattering of light on gold nanoparticles both theoretically and experimentally. We modeled resonance phenomenon using Mie scattering theory and, have shown that our model agrees with our experimental results.

The future work will use these results to fabricate the nanocavity with a number of periodic corrugations around the center slit for obtaining a highly directional emission of light. These nanostructures can be applied to experimental cavity quantum electrodynamics phenomenon and development of single -photon sources.

APPENDIX A

MATLAB PROGRAMS

A. MATLAB PROGRAMS FOR SIMULATING MIE SCATTERING BY GOLD NANOPARTICLES

```
.
clc
clc
close all
clear all


% Gold dielectric constant polyfit----------Begin----------
 f=load('gold.txt');                          %Gold dielectric values in the file gold.txt
reall=f(:,1);
imaginaryy=f(:,2);
x=1:0.2:25;
%m1=polyfit(x,reall',15)
%o1=polyval(m1,x)
%m2=polyfit(x,imaginaryy',15);
%o2=polyval(m2,x);

 hreal=       -0.00000005389646*x.^9+                0.00000662599218*x.^8          -
0.00034092766348*x.^7+   0.00951412248213*x.^6 ...
  -0.15610767041776*x.^5+       1.52916615978011*x.^4     -8.70652493622014*x.^3+
26.72323467165262*x.^2 ...
 -39.20216937129737*x+  19.99188460820344;
himaginary=      -0.00000000855552*x.^9+           0.00000099136209*x.^8          -
0.00004823565729*x.^7 +  0.00127677403818*x.^6 ...
  -0.01985835281469*x.^5+       0.18187845997255*x.^4     -0.91889363073050*x.^3+
2.17866863634756*x.^2 ...
   -2.33201315694188*x+   7.64528440730163;

%-----------------------------------------------------------End--------------------

%Actual program-----------------------------

 wavelength=300e-9:10e-9:1500e-9;                %Wavelength span of interest
 d=1;                          %This is an index for referring to dielectric constant(gold)
array
 theta1 = 56-(2*180);%In degree

 theta = theta1*pi/180;
 f=[];
for a = 1e-9*[20,50,80,100]            % Simulation for four different nanosphere radii
(First "for" loop)
```

```
tot=[];                                                    %Initial value.
sumI=[];                                                   %Initial value.
for lambda= wavelength                                  % Second "for" loop



 r=10;                                                  %far fileld approximation (in meters)
   q=2*pi*a/lambda;
   c=3e8;
   w=2*pi*3e8./lambda;

   wc=2*pi*6.5e12;                                % constants for gold dielectric permittivity
   wp=2*pi*2.175e15;                          %in the IR/visible region by Lorentz relation

   beta=1e14;                                                %damping factor for gold
   m=9.1e-31;
   N=m*(wc^2+beta^2)./(4*pi*(1.6e-19).^2);

   sigma=                                45210000;%N*(1.6e-19).^2./(m*(beta-i*w));%Gold
conductivity(frequency dependent factor)


  %45210000;                                              %conductivity of gold
   %eps12=1-(wp^2./(w.*(w+i*wc)))+8i;%8i is added to convert the model from ir to
visible
   eps1=1;                                                  %dielectric constant of air

    hreal = -0.00000005389646*x.^9+ 0.00000662599218*x.^8 -
0.00034092766348*x.^7+  0.00951412248213*x.^6 ...
 -0.15610767041776*x.^5+ 1.52916615978011*x.^4  -8.70652493622014*x.^3+
26.72323467165262*x.^2 ...
 -39.20216937129737*x+  19.99188460820344;%Real value of gold dielectric
constant(polynimial fit)



himaginary = -0.00000000855552*x.^9+ 0.00000099136209*x.^8 -
0.00004823565729*x.^7 +  0.00127677403818*x.^6 ...
 -0.01985835281469*x.^5+ 0.18187845997255*x.^4  -0.91889363073050*x.^3+
2.17866863634756*x.^2 ...
 -2.33201315694188*x+  7.64528440730163;%Imaginary value of gold dielectric
constant(polynimial fit)
```

```
    eps12(d)=hreal(d)-i*himaginary(d);

     k12(d)=(i*2*pi/lambda)*(eps12(d)+i*4*pi*sigma/w);%constant required (from
Born and Wolf)
     k1=i*(2*pi/lambda)*eps1;                    %constant required (from Born and
Wolf)
     nsqr(d)=(k12(d)/k1); % n^2
     n(d) = sqrt( nsqr(d) );
    n=n(d);                                              %refractive index

  a=q*(lambda/(2*pi));                                   %radius of the nano sphere
   n1=5;                                               %Legendre summation numbers


   c=3e8;
   w=2*pi*3e8./lambda;
   %Bessel function value calculation,  defined as functions ---Begin------------------

  for l=1:n1
        cons = i^(l+1)*(2*l + 1)/(l*(l+1));
     nr = n*riccati_bessel_deriv(l,1,q)*riccati_bessel(l,1,n*q) ...
        - riccati_bessel(l,1,q)*riccati_bessel_deriv(l,1,n*q);
     dr = n*riccati_hankel_deriv(l,1,q)*riccati_bessel(l,1,n*q) ...
        - riccati_hankel(l,1,q)*riccati_bessel_deriv(l,1,n*q);
     eB(l) = cons.*nr./dr;

     nr = n*riccati_bessel(l,1,q)*riccati_bessel_deriv(l,1,n*q) ...
        - riccati_bessel_deriv(l,1,q)*riccati_bessel(l,1,n*q);
     dr = n*riccati_hankel(l,1,q)*riccati_bessel_deriv(l,1,n*q) ...
        - riccati_hankel_deriv(l,1,q)*riccati_bessel(l,1,n*q);
     mB(l) = cons.*nr./dr;

          %--------------------------------End-------------------------------



   %intensity calculations

     pl=legendre(l,cos(theta));

     pl1_deriv = (l+1)*l*(cos(theta)^2-1)^0.5*pl(1)-cos(theta)*pl(2);
```

```
    P11(l) = pl1_deriv(1)*sin(theta);
    P12(l) = pl(1)/sin(theta);

    P21(l) = pl(1)/sin(theta);
    P22(l) = pl1_deriv(1)*sin(theta);
    Ipar(l)=abs((lambda^2./(4*pi^2*r^2)).*(-i)^l*(eB(l).*P11(l)-mB(l).*P12(l))).^2;
    Iper(l)=abs((lambda^2/(4*pi^2*r^2))*(-i)^l*(eB(l)*P21(l)-mB(l)*P22(l)))^2;
  %------------------------------

 end


sumI=[sumI,sum(Iper)];  %Ipar is summed up and final value joins sumI. Basically this
is array concatenation.
  tot=[tot,sum(Iper)];%Similar to the above one

t=tot;

end
I = abs(4*pi*pi*a^2*(tot))/1e-45;        %Final scattered light intensity. I divided by a
factor of 1e-45.
d=d+1;                                                %gold array incrementation
plot(wavelength,I)
hold on
grid on

end

Calculation of riccati_hankel functions of 1st, 2nd kind.
%
function v = riccati_hankel( order, kind, z )
    v = sqrt(pi*z./2)*besselh(order+0.5,kind,z);
end

Calculation of riccati_hankel first derivativ functions of 1st, 2nd kind.
%
function v = riccati_hankel_deriv( order, kind, z )
    v = sqrt(pi./(8*z))*besselh(order+0.5, kind, z) + ...
       sqrt(pi*z./2)*(besselh(order-0.5,kind,z) ...
       -( order + 0.5).*besselh( order + 0.5, kind, z )./z );
end

Calculation of riccati_bessel functions of 1st, 2nd kind.
%
```

```
function v = riccati_bessel( order, kind, z )
   if ( kind == 1 )
      % calculate S
      v = sqrt(pi*z./2)*besselj(order+0.5,z);
   elseif ( kind == 2 )
      % calculate C
      v = -sqrt(pi*z./2)*bessely(order+0.5,z);
   else
      error('unknown kind');
   end
Calculation of first derivative of riccati bessel function
function v = riccati_bessel_deriv( order, kind, z )
   if ( kind == 1 )
      % calculate S
      v = sqrt(pi./(8*z))*besselj(order+0.5,z) + ...
         sqrt(pi*z./2)*(besselj(order-0.5,z) - (order + 0.5).*besselj(order+1/2,z)./z);
   elseif ( kind == 2 )
      % calculate C
      v = -sqrt(pi./(8*z))*bessely(order+0.5,z) + ...
         -sqrt(pi*z./2)*(bessely(order-0.5,z) - (order + 0.5).*bessely(order+1/2,z)./z);
   else
      error('unknown kind');
   end
end
```

REFERENCES

[1] T.W. Ebbesen, H.J. Lezec, H.F. Ghaemi, T. Thio and P.A.Wolff: "Extraordinary optical transmission through sub-wavelength hole arrays", Nature **391** (6668), 667–669 (1998) .

[2] C. F Bohren, , D. R Huffman, "Absorption and scattering of light by small particles,ed" Wiley, New York, 1983.

[3] H. J. Lezec, A. Degiron, E. Devaux, R. A. Linke, L. Martin-Moreno, F. J. Garcia-Vidal, and T. W. Ebbesen, "Beaming light from a subwavelength aperture," science **297**, 820 (2002)

[4] J.-M. Gerard and B. Gayral, "Strong Purcell effect for InAs quantum boxes in three- dimensional solid-state microcavities", IEEE Journal of Lightwave Technology, **Vol. 17**, No. 11, pp. 2089-2095 (1999).

[5] L. Martin-Moreno, F. J. Garcia-Vidal, H. J. Lezec, A. Degiron, and T. W. Ebbe-sen, "Theory of highly directional emission from a single subwavelength aperture sur- rounded by surface corrugations," Phys. Rev. Lett. **90**, 167401 (2003).

[6] F. J. Garcia-Vidal, H. J. Lezec, T. W. Ebbesen, and L. Martin-Moreno, "Multiple paths to enhance optical transmissions through a single sub wavelength slit," Phys.Rev. Lett. 90, 213901 (2003).

[7] M. Vasilyev and P. Kumar, "Efficient coupling between Gaussian cavity mode and metal nanoaperture," *NanoPhotonics in Information Sciences conference*,San Diego,CA, April 2005, paper NWB4.

[8] M.Annamali, S. C. samudrala and M.Vasilyev, "Optimization of coupling between metal nanocavity and a free space Gaussian mode",*CLEO/QELS (Quantum Electronics and Laser Science) conference* ,sanjose,CA,May 2008.

[9]. M. Annamali, "Optimization of coupling from a sub wavelength metal nanoaperture to a Gaussian mode," MS Thesis, Dept of Electrical engineering, University of Texas at Arlington,2007.

[10] M. Born and E. Wolf, *Principles of Optics*, 7th edition, Cambridge University Press.

[11] S. Ramo, J. R. Whinnery and T. V. Duzer, *"Fields and waves in Communication electronics"*, 2nd edition, John Wiley & Sons, Newyork, 1984.

[12] Donald L. Smith. "*Thin-film deposition : principles and practice*", McGraw-Hill Professional; 1 edition.

[13] M. L. Brongersma, P.G. Kik, *Surface plasmon nanophotonics* (Springer Series in Optical Sciences).

[14] C. E. Rayford II , G. Schatz, K.Shuford, "Optical properties of gold nanospheres" **Vol 2**, Issue 5, Spring 2005, Nanoscape.

BIOGRAPHICAL INFORMATION

Sarath Chandra samudrala got his M.Sc(Tech)in Physics(Fiber optics) from Jawaharlal Nehru Technological University, Hyderabad, India. After a brief period of working on the development of fiber optic gyroscopes he came to USA and earned M.S in Physics from University of Texas at Arlington in year 2008. His research interests include fiber optics, nonlinear optics, quantum optics and cavity quantum electrodynamics.